ADVANCED PHOTONICS RESEARCH
Open Access
www.adpr-journal.com

Revealing Two Operation Modes of Perovskite Light-Emitting Diodes Through Overshoot Pulses

*Rokas Gegevičius, Ignas Ledzinskas, Jevgenij Chmeliov, Iakov Goldberg, Robert Gehlhaar, Karim Elkhouly, and Vidmantas Gulbinas**

In some applications, perovskite light-emitting diodes (PeLEDs) shall operate in pulsed mode. The generation of high-intensity light pulses requires PeLED driving by high-power electrical pulses, which can lead to deterioration of PeLED performance and their degradation. Contrarily, PeLEDs operating in a nonconventional regime, based on the so-called overshoot effect, enable the generation of short, high-intensity optical pulses at relatively low driving pulse power. Here, the generation of overshoot pulses (OSPs) by FAPI PeLEDs is analyzed. The intensity and shape of the OSPs are determined not only by the driving (injection) pulse parameters but also by the offset voltage applied between the injection pulses and the afterpulse applied after the injection pulse. The offset voltage determines the distribution of the mobile ions, which strongly affect the internal electric field during the pulse action and after its termination, thus strongly affecting the evolution of the conventional electroluminescence (EL) and generation of the OSPs. Meanwhile, the afterpulse voltage controls the intensity and duration of the OSPs. The intensity of the OSPs increases strongly at temperatures below ≈200 K. Mathematical modeling reproduces the EL dynamics and reveals two distinct PeLED operation modes: one that facilitates OSP generation and another that prevents it.

1. Introduction

Although metal halide perovskites are attracting the most attention as materials for the next-generation solar cells, remarkable success has also been achieved through their application in other electro-optical devices,[1] including light-emitting diodes (LEDs).[2–5] Perovskite LEDs (PeLEDs) may be formed directly on electronic boards and on flexible substrates, which makes them particularly interesting for flexible electronics. The chemical and morphological diversity of perovskites enables the tuning of PeLED luminescence in the entire visible and near-infrared spectral range, resulting in high luminescence quantum yield and brightness. PeLEDs now show excellent external quantum efficiencies of up to 30%.[6–10] In addition to their use for lighting and displays, where PeLEDs operate in quasistable mode, there are also many applications, where pulsed operation of PeLEDs is desirable, e.g., in communication, triggering and sensing. Although very high-intensity pulsed PeLEDs have been demonstrated with record luminance close to, or even exceeding Mcd/m^2,[11–13] these devices operate at very high current densities of up to $\approx 1\ kA\ cm^{-2}$. This poses a challenge for conventional electronics and also for PeLEDs, leading to their rapid degradation and damage. In addition, the generation of short electric pulses is limited by the capacitance of the device and by some electronic processes in PeLEDs that affect the rise and decay rates of electroluminescence (EL).

We have recently demonstrated that short EL pulses may be generated in an unconventional regime based on the so-called overshoot effect, in which a short EL peak is observed immediately after the end of the injection pulse.[14] The overshoot effect was also previously observed in organic LEDs.[15,16] Overshoot peaks with intensities significantly exceeding intensity of conventional EL have been reported for perovskite devices with solar cell[14] and PeLED[17,18] architecture.

Briefly, the mechanism for the formation of overshoot pulses (OSP) is as follows. When a bias voltage is applied to the PeLED, charge carriers are injected into the active layer and recombine to produce EL. In certain operating regimes, however, some of the charge carriers cross the active layer and accumulate next to the

R. Gegevičius, I. Ledzinskas, J. Chmeliov, V. Gulbinas
Center for Physical Sciences and Technology
Sauletekio Ave. 3, Vilnius LT-10257, Lithuania
E-mail: vidmantas.gulbinas@ftmc.lt

The ORCID identification number(s) for the author(s) of this article can be found under https://doi.org/10.1002/adpr.202500190.

DOI: 10.1002/adpr.202500190

J. Chmeliov
Institute of Chemical Physics
Faculty of Physics
Vilnius University
Sauletekio Ave. 9, Vilnius LT-10222, Lithuania

I. Goldberg, R. Gehlhaar, K. Elkhouly
IMEC
Leuven 3001, Belgium

opposite electrode. The recombination of the accumulated charge carriers is inefficient, as electrons and holes are spatially separated from each other. However, when the applied voltage is switched off, the internal electric field disappears, allowing the electrons and holes to diffuse towards each other, resulting in their recombination and generation of an intense EL pulse. Consequently, the device can be driven for a relatively long time with a low power electric current, leading to an accumulation of charge carriers, and generates a short high-power optical pulse when the electric injection pulse ends, which also ensures perfect electrical synchronization.

The overshoot-based devices would be very attractive for their integration into conventional and more advanced flexible plastic electronics currently under active development, including portable electronics with limited power supplies. Low-power, low-voltage electrical injection pulses can generate short, high-intensity light pulses. Perovskites with different band gaps could enable the production of PeLEDs of different colors. This PeLED operation concept can probably also be applied to other types of LEDs, such as organic LEDs and LEDs based on some nanostructures or even on conventional semiconductors. This design concept for high-power pulsed PeLEDs could also be attractive for the developing electrically pumped perovskite lasers, which have not yet been demonstrated. The high-power pumping required for lasers leads to electrical damage, heating, and other problems. Low-power pumping, enabled by the overshoot effect, is therefore a very attractive alternative.

However, the properties of the OSPs and the optimization of their intensity and duration have not yet been systematically investigated. Therefore, the potential of this technique still remains unclear. Consequently, overshoot is still considered as an interesting effect with unclear application perspectives. Here, we investigate the formation of OSP in formamidinium lead iodide (FAPI) PeLEDs optimized for pulsed performance. We mainly focus on the operation conditions of the PeLEDs and show that the OSP generation and its characteristics strongly depend on the variations of the driving voltage. We demonstrate two PeLED operation modes: one enables OSP generation, while the other inhibits it but is more favorable for conventional EL.

2. Results

2.1. Experimental Results

2.1.1. Dependence of the EL Dynamics on Injection Pulse and Offset Voltages

Here, we investigated FAPI PeLEDs with a FAPI layer thickness of about 40, 120, and 160 nm. We mainly focused on the 40 nm device, which showed the best results under high-voltage pulsed driving and was carefully optimized for pulsed operation. Depending on the driving voltage, its external quantum efficiency reaches 10% at several hundred mA/cm^2.[19] We begin the discussion of our experimental data by analyzing the performance of PeLEDs with different perovskite layer thicknesses at different electrical driving regimes (shown in **Figure 1**a) at room temperature.

Figure 1b shows the dynamics of the EL of the 40 nm device during driving with rectangular pulses of 20 µs duration and different voltages at a repetition rate of 6.6 Hz (here, no offset voltage and no afterpulse were applied). The EL signal grows during the initial ≈3 µs and then increases slightly additionally during the remaining injection pulse. An OSP was not observed at any of the applied voltages. However, the OSP was clearly visible when a negative offset voltage of −2.5 V was applied during the time intervals between the injection pulses (Figure 1c). Although the absolute OSP intensity increased with injection pulse voltage, the relative OSP intensity compared to the intensity of the normal EL was highest at the lowest pulse voltage of 3 V. Figure 1d shows the EL dynamics for the 40 nm device at different offset voltages. With increasing negative offset voltage, the intensity of the OSP first increased but then started to decrease again when the offset voltage exceeded −3 V.

The offset voltage changes not only the OSP intensity but also the intensity and growth dynamics of the conventional EL signal. At zero offset voltage, we observe rapid PL growth, especially at high injection voltages. This growth time of about 3 µs roughly corresponds to the *RC* characteristics of the driving circuit; thus, we can assume that the EL arises immediately when the sample capacitance is charged and the voltage across the diode reaches the voltage supplied by a generator. On the other hand, Figure 1c, d shows that the EL growth was much slower when the negative offset voltage was applied and was especially slow at high negative offset voltages. The delayed EL growth was also reported in previous publications together with the slow growth of the injection current and was attributed to the redistribution of ions changing the carrier injection rate.[20] However, this dynamics took place on a time scale of milliseconds and seconds, which is typical for the redistribution of ions.[21,22] In our case, the initial current was strongly dominated by the capacitive current. **Figure 2** shows the total current dynamics under +1 and −1.5 V offset values and the growth dynamics of the evaluated injection current obtained after subtracting the capacitive current, which was considered being identical, only of opposite sign, as that observed after the injection pulse termination.

The injection current kinetics at positive and negative offsets are very similar, except for the ≈2 µs delay observed in the latter case. This time delay corresponds to the growth of the voltage applied to the device from −1.5 to +1 V during charging of its capacitance. This delay also explains the delayed switch-on of the EL at negative offset but cannot explain the much slower subsequent EL growth during more than 10 µs. Consequently, some additional process is responsible for this process.

Figure 3 illustrates the basic processes responsible for the slow EL growth during the electrical injection pulse and OSP formation after the injection pulse termination. The figures on the left show band diagrams before the injection voltage is applied at different offset voltages. The permanently applied offset voltage, together with the built-in electric field created by the different work functions of the electrodes, causes a redistribution of the mobile ions, which in turn creates its own electric field that partially shields the applied offset field. When injection voltage is applied (middle figures), electrons and holes are injected into the perovskite layer and drift through it under the influence of the internal electric field created by both the applied voltage and the redistributed ions. During their drift, some charge carriers recombine and cause EL, while others traverse the perovskite layer and accumulate at the opposite side, being unable

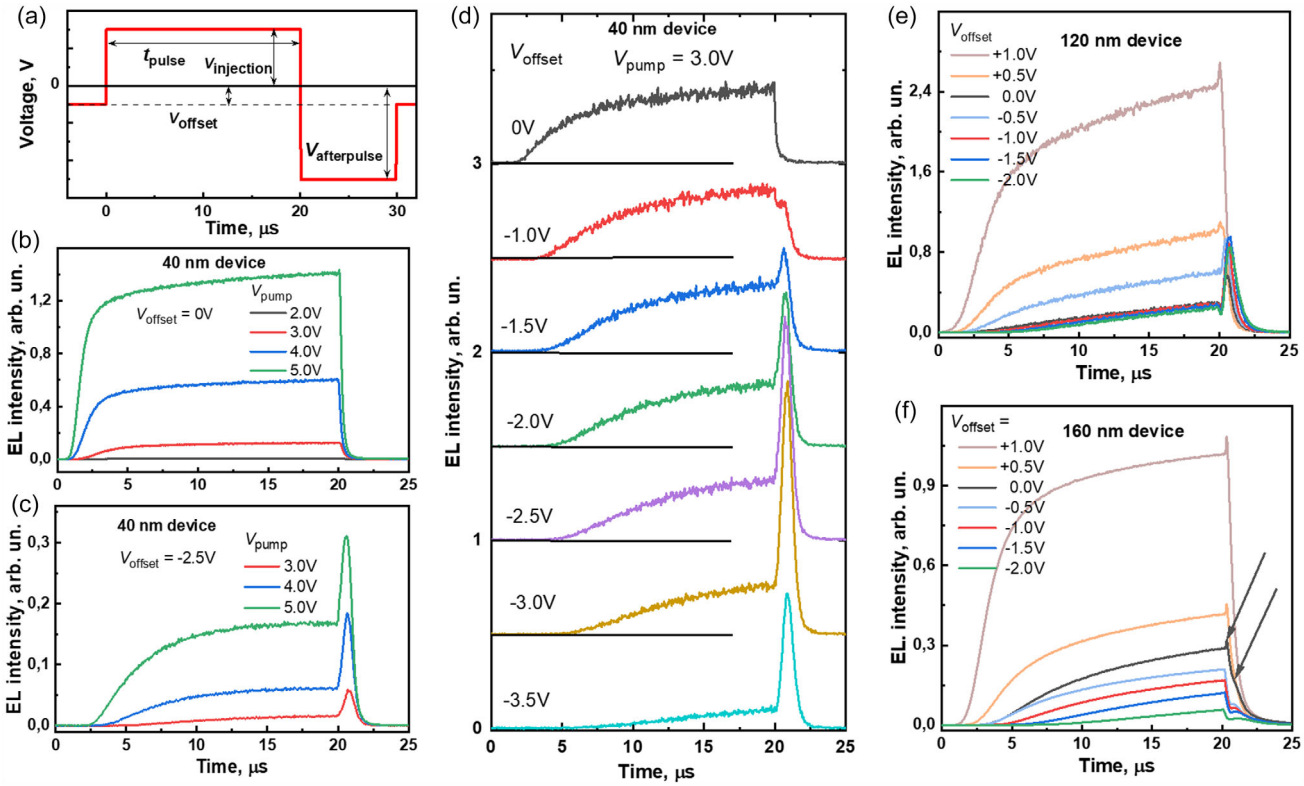

Figure 1. PeLED driving voltage time chart. a) EL dynamics of PeLEDs driven with 20 μs long electrical pulses at a repetition rate of 6.6 Hz b–f). b,c) show the EL dynamics for 40 nm PeLED at different injection pulse voltages at an offset voltage of 0 V (b) and −2.5 V (c). (d–f) show the dependencies of the EL dynamics on the offset voltage when driving with 3 V pulses for d) 40 nm, e) 120 nm, and f) 160 nm PeLEDs. Arrows in plot (f) show two types of OSPs (see text for details).

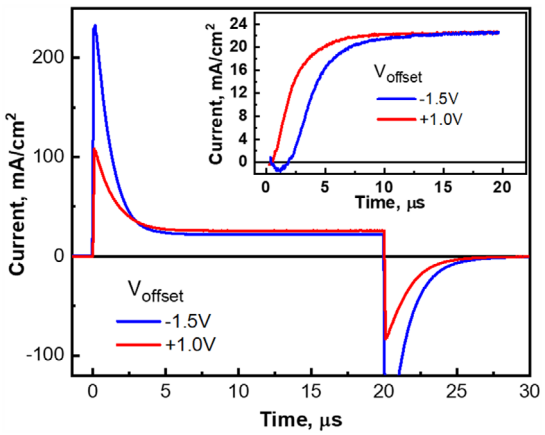

Figure 2. Current dynamics in 40 nm PeLED, created by 3 V injection pulses under +1 V (red line) and −1.5 V (blue line) offset voltages. The inset shows injection current, obtained by subtracting the capacitive current.

to cross the blocking layers. At the end of the injection pulse, the electric field disappears or even reverses due to the applied offset voltage, causing move back of all the accumulated charge carriers driven by drift and diffusion (right figures). During this process, they recombine with the opposite charge carriers moving from the other side, which results in the formation of the OSP.

The movement of the ions takes place on a time scale of milliseconds, so that their positions and, thus, their created secondary electric field do not change during the injection pulse. In the case of a positive offset voltage, the secondary field of ions reduces the electric field of the injection pulse. The weakened electric field reduces the drift velocity of the charge carriers; thus, they recombine before crossing the perovskite layer. In this case, recombination starts immediately after the injected electrons and holes have crossed about half of the perovskite layer thickness and meet each other, which takes nanoseconds at most. Thus, when observed in the microsecond range, the EL appears immediately after the sample capacitance is charged, which is consistent with the data shown in Figure 1b. Most charge carriers recombine before crossing the perovskite layer, so they do not accumulate and do not cause OSP formation.

In the opposite case of a negative offset, the ionic field enhances the electric field of the injection pulse, so that the charge carriers move faster. As a result, they cross the perovskite layer more quickly, which reduces the probability of recombination and results in weaker conventional EL (Figure 1d). Finally, charge carriers accumulate next to the opposite electrodes, preparing a favorable carrier distribution for the formation of OSP. Intense EL begins only when large carrier densities accumulate, and the injected carriers of the opposite sign recombine with the accumulated carriers. The EL increases dramatically as OSP when the electric field terminates and the recombination of both signs

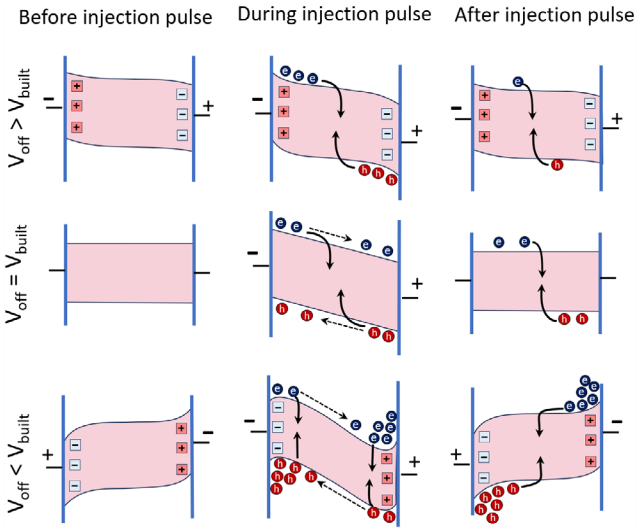

Figure 3. Schematic illustration of the PeLED performance at different offset voltages V_{off} compared to the built-in voltage V_{built}. Red and blue squares illustrate accumulation of the mobile positive and negative ions (or the corresponding vacancies) next to the electrodes, and circles depict the dynamics of free electrons and holes, followed by their recombination; see text for details.

accumulated charge carriers begins. Thus, this model suggests that the growth of conventional EL intensity and the formation of OSP are interrelated, in agreement with the experimental data. Similar correlation between EL growth and OSP formation could be also observed in experimental data presented in refs. [18,23]. Moreover, this model predicts the existence of two PeLED operation modes with different spatial carrier distributions and different EL dynamics. We refer to them as recombination and accumulation modes. As Figure 1c shows, one can switch the device performance between the two modes by changing the offset voltage. The accumulation mode, sometimes called as overflow regime, has been investigated in several papers in relation to carrier leakage and efficiency roll-off.[24,25]

The EL dynamics in thicker devices, shown in Figure 1e,f, reveals other important features. First, at high offset values, a slight decrease in EL intensity is observed immediately after the termination of the electrical injection pulse. This feature is consistent with the presented model: the termination of the injection pulse stops the injection of new charge carriers and their recombination, observed as a conventional EL, and it takes some time for the accumulated electrons and holes to move towards each other and facilitate their recombination, resulting in an OSP. The second new feature is the appearance of a very short, low-intensity OSP even at positive and zero-offset voltages. This pulse appears immediately after the termination of the injection pulse, while the more intense and longer OSP observed at higher negative offset voltages appears with a delay of about 1 μs. The 160 nm device showed both OSPs at 0 V offset voltage, as indicated with arrows in Figure 1f. Thus, we observe two types of OSPs: strong delayed OSPs occurring at negative offsets and weak instantaneous OSPs manifesting itself at positive or zero offset voltages. The instantaneous OSPs are apparently overtaken by the stronger delayed OSPs at negative offsets.

The formation of the instantaneous OSPs is not predicted by the model described above. We attribute them to the separation of electrons and holes within individual perovskite grains. In our previous work on electric field-induced luminescence quenching, we identified two kinds of the electric field-induced spatial separations of electrons and holes causing luminescence quenching: separation of electron and hole clouds within the perovskite layer and separation of charge carriers within individual perovskite grains.[21] The latter type of separation disappears very quickly after the termination of the electric field, determined by the diffusion of charge carriers within a single monocrystalline perovskite, which, according to reported diffusivity values, is expected to occur on a picosecond timescale. Consequently, termination of the field-induced luminescence quenching taking place much faster than our time resolution leads to the increase of the luminescence intensity observed as an instantaneous OSP. The duration of this OSP is determined by the recombination of electrons and holes inside individual perovskite grains, which also typically takes place on a nanosecond time scale. The instantaneous OSPs are, however, very weak and, thus, hardly practically important; therefore, next, we will focus only on the more intense delayed OSPs.

2.1.2. Dependence of the EL Dynamics on Afterpulse Voltage

In order to additionally manipulate the conditions of OSP formation, we have introduced an additional 10 μs long electrical pulse immediately after the end of the injection pulse, which we call the afterpulse (see Figure 1a). The afterpulse has no influence on the charge carrier dynamics and accumulation during the injection pulse or on the distribution of the ions. It only changes the OSP formation by altering the movement of the accumulated charge carriers. **Figure 4** shows the influence of the afterpulse voltage.

As expected, the accumulated charge carriers move faster towards each other when the negative afterpulse value is increased, causing the OSP to narrow and shift towards shorter times. The shift is more noticeable in thicker devices, where the accumulated charge carriers need more time to move and recombine. However, the time-integrated OSP value does not change significantly, as this value is determined by the number of accumulated charge carriers, most of which subsequently recombine regardless of the afterpulse voltage. Interestingly, when the afterpulse ends, it leads in some cases to the formation of the second OSP (see Figure 4b). The mechanism for the formation of the second OSP is similar. Positive afterpulse only diminishes the positive electric field without changing its direction. Therefore, only diffusion drags clouds of accumulated charge carriers towards each other, while electric field of the positive afterpulse still keeps them apart. When it is terminated, the accumulated charge carriers move faster towards each other and recombine, forming a second afterpulse.

2.1.3. Dependence of the EL Dynamics on Injection Pulse Duration

Since the accumulation of the charge carriers takes place during the injection pulse, its duration should be an important

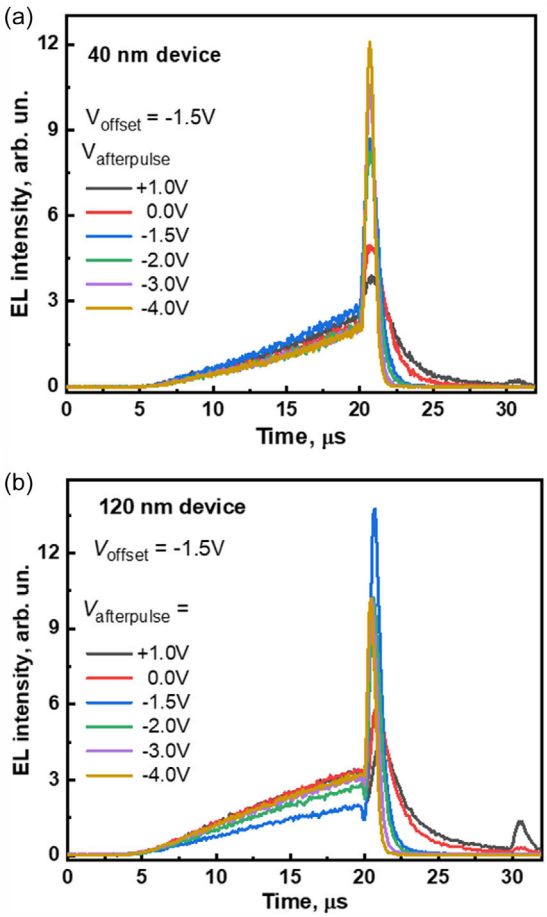

Figure 4. OSP formation in 40 nm a) and 120 nm b) devices at 4 V injection pulses, −1.5 V offset, and different afterpulse voltages.

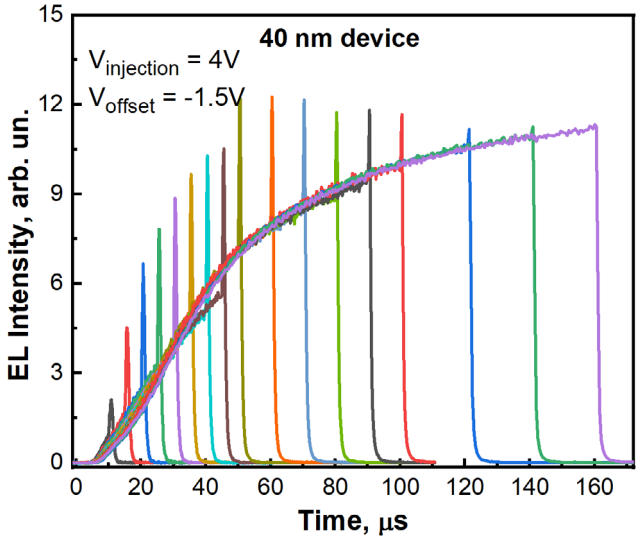

Figure 5. OSP formation at different injection pulse durations obtained for 40 nm sample at 4 V injection and −1.5 V offset voltages. No afterpulse was applied.

parameter determining OSP properties. **Figure 5** shows the EL development and OSP formation at different injection pulse durations.

The OSP intensity (above the conventional EL intensity) increases until the pulse duration reaches 20–30 μs and saturates for longer pulses. After about 60 μs, it starts to decrease again and gradually disappears when the pulse duration reaches ≈160 μs. A similar dependence was also reported in ref. [23] and was attributed to different distributions of mobile ions caused by different duty cycles, i.e., ratios between the injection pulse duration and the full period of alternating voltage. However, the experimental conditions were very different as the diodes were driven at a frequency of 1 kHz and a pulse durations ranging from 100 to 900 μs. The duty cycles were therefore between 10 and 90%. In our experiments with 6,6 Hz pulse frequency, the duty cycle was only between 0.0066% and 0.1%. The injection voltage was therefore only present for a negligible fraction of the time. Therefore, it is unlikely that it could significantly alter the ion distribution and affect the performance of the device. Furthermore, the rise of the conventional EL becomes very long as the duration of the injection pulse increases, which in contrast is indicative of the accumulation mode. These contradictions suggest that some additional process, rather than ion redistribution, causes the disappearance of the OSP. Based on these features, we hypothesize that the observed dynamics may be caused by the population of trap states. During the operation of the device in the accumulation mode, accumulated charge carriers can be trapped by the trap states, whereby the accumulated mobile charge carriers are gradually replaced with trapped charge carriers, which are immobile and do not recombine radiatively and thus cannot form OSP. On the other hand, the accumulated carriers shield the internal electric field in a similar way as ions redistributed by the positive offset voltage and gradually shift the device performance to the recombination mode, which is more favorable to the conventional EL, leading to a gradual increase in EL intensity. Thus, both processes, ion redistribution and population of trap states, cause very similar consequences, but their roles are expected to strongly depend on the particular material properties, namely the presence and concentrations of mobile ions and trap states as well as their properties.

2.1.4. EL Dynamics at Low Temperatures

To obtain additional information about the electronic processes during pulsed PeLED driving, we also analyzed the EL dynamics at different temperatures. The investigations were carried out at an offset voltages of +1 and −1.5 V, which were applied at the start of cooling of the device and maintained continuously during cooling and measurements. This allowed us to ensure an identical spatial ion distribution and thus an identical shielding of the applied electric field at all temperatures used. It has been shown that such a regime with a positive offset voltage ensures a higher conventional EL efficiency than the regime where the offset voltage was applied after the device was cooled.[26] In the latter case, the redistribution of ions was hindered or completely prevented at low temperatures, resulting in weaker shielding of the applied electric field.

No significant changes of the EL dynamics were observed by lowering the temperature to 15 K while keeping a constant offset voltage of +1 V (**Figure 6**a). Cooling the sample only led to a slight increase in EL intensity. However, considering that the injection current decreased more than two times at temperatures below 100 K (see insert in Figure 6a), the efficiency of the device increased significantly, in agreement with previous reports,[26] mainly attributed to the higher radiative recombination rates in perovskites at low temperatures.[27,28] The OSP, which was not observed at RT, became easily visible at low temperatures. The resulting OSP was very short, much shorter than the one observed at room temperature with negative offset, so it is more likely to be of the instantaneous type, as described above. The occurrence of the instantaneous OSP can be surmised at low temperatures, as weaker carrier diffusion and a stronger influence of the grain boundaries should result in a stronger field-induced separation of electrons and holes within the grain.

Cooling the sample at an offset of −1.5 V also led to a reduction in current, an increase in conventional EL intensity and, thus, to an increase in device efficiency. In general, device efficiency is determined by the competition between radiative recombination and the nonradiative losses caused by nonradiative recombination and carrier leakage. Charge carrier leakage is apparently less important at positive offset voltages when the absence of overshoot indicates that the accumulation of charge carriers next to the opposite electrodes is insignificant or absent. However, at negative or even zero offsets, the reduction in leakage may be an important factor increasing EL intensity at low temperatures. Additional factors may also be reduced monomolecular and increased bimolecular recombination rates at low temperatures as demonstrated for the conventional $MAPbI_3$ perovskites.[29]

The OSP intensity at negative offset voltages increases dramatically at low temperatures. The simple explanation for this is a reduction in charge carrier leakage. On the other hand, some other material parameters may become more favorable for overshot formation at low temperatures, such as a reduced carrier trapping rate or changes in carrier motion parameters, which are discussed in the following.

2.2. Mathematical Modeling

To gain a better insight into the electronic processes in PeLEDs, we modeled the performance of the devices. We used a similar approach as in our previous publication, where we analyzed the overshoot effect in the perovskite solar cell architecture.[14] Briefly, coupled Einstein−Smoluchowski diffusion equations were used to describe time-dependent distributions of charge carriers within the perovskite layer

$$\frac{\partial n}{\partial t} = \frac{\partial}{\partial x}\left[-v_n n + D_n \frac{\partial n}{\partial x}\right] - \gamma np \tag{1}$$

$$\frac{\partial p}{\partial t} = \frac{\partial}{\partial x}\left[-v_p p + D_p \frac{\partial p}{\partial x}\right] - \gamma np \tag{2}$$

where the drift velocities $v_{n(p)}$ and diffusion coefficients $D_{n(p)}$ for electrons (holes) are related to their mobilities $\mu_{n(p)}$: $v_n = -\mu_n E$, $v_p = \mu_p E$, and $D_{n(p)} = \mu_{n(p)} k_B T/e$; here, E denotes the strength of the internal electric field, $k_B T$ is thermal energy, and e is elementary charge. The luminescence intensity was described as a result of bimolecular electron and hole recombination (the last terms in Equations (1) and (2), with γ being the recombination rate constant); thus, it was considered to be proportional to the product of the electron and hole densities, integrated over the perovskite layer thickness

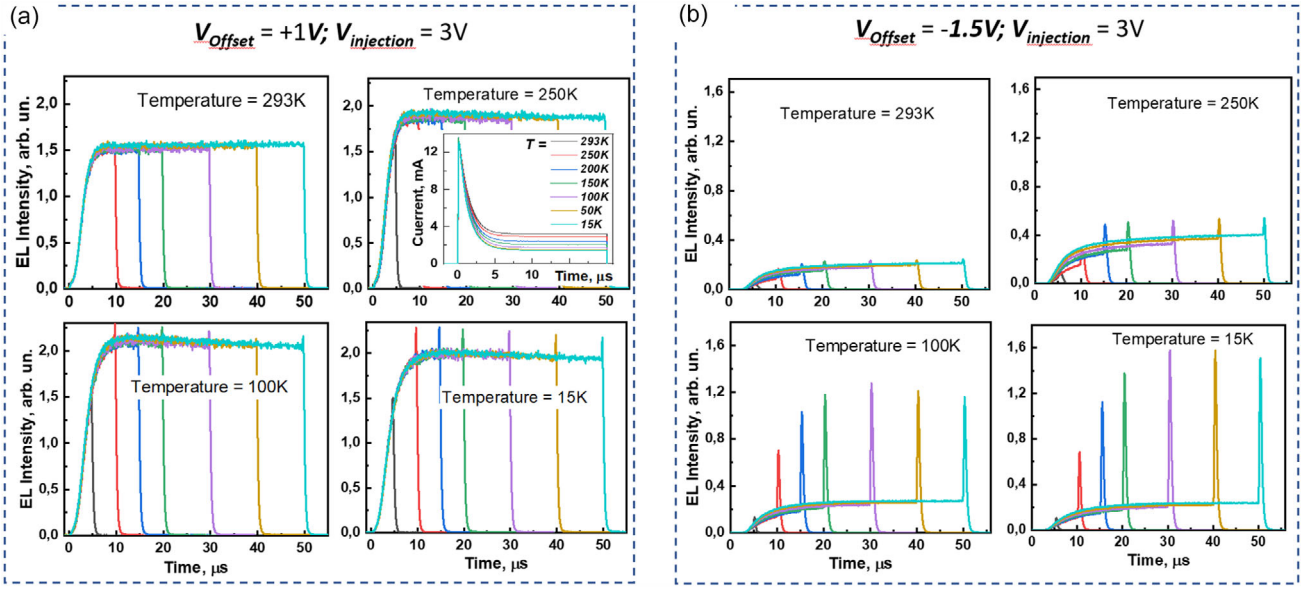

Figure 6. EL dynamics of 40 nm PeLED at different temperatures, obtained by electrical driving with 3 V electrical pulses of different durations under +1 V a) and −1.5 V b) offset voltages applied constantly during the device cooling and measurements. Insert in (a) shows current transients at different temperatures. Temperature values correspond to those set by cryostat. Real temperature of PeLED could be higher than the setpoint, particularly at 15 K.

$$\mathrm{EL}(t) \propto \int \gamma n(x,t)p(x,t)\,\mathrm{d}x \tag{3}$$

For the sake of simplicity, here, we assumed that ions, screening the external electric field, accumulate within very thin surface layers; thus, their electric field is homogeneous across the perovskite layer. This is justified by thin perovskite films and strong negative offset voltages causing ion redistribution. According to our previous estimations,[14] the typical thicknesses of ion "clouds" shall be of several nanometers only. For simplicity, we also assumed that electrons and holes have identical properties (except charge); thus, the obtained distributions $n(x)$ and $p(x)$ were symmetric to each other.

Several parameters of the device, such as carrier mobility, diffusivity, recombination rate, and internal electric field, are also poorly known. Here, we have assumed that the electric field created in different layers of the device by the negative applied voltage in the absence of current is inversely proportional to the dielectric constant of the layer. According to this estimate, about 10% and 30% of the applied voltage drops on perovskite layers of 40 and 120 nm devices, respectively. Estimating the electric field strength during the injection pulse, when an injection current is present and the redistributed ions create an additional internal field, is even more difficult. When current flows through the device, the voltage drop across the perovskite layer is determined by the conductivities of the perovskite and transport layers, which are determined by the charge carrier densities and their mobilities. Therefore, the internal electric field strength was used as an adjustable parameter.

Carrier mobilities in organic and PCBM transport layers are considered to be much lower than in the perovskite layer, meaning that only a small part of the applied injection voltage drops on the perovskite layer. The internal electric field within the perovskite is further shielded by mobile ions and trapped charge carriers. Therefore, the electric field strength was a free parameter in our simulations to achieve the best agreement with the experimental data. We estimated the internal electric field strengths from the experimental data, assuming that the internal field created by the ions is proportional to the offset voltage, while the field created by the injection or afterpulses is proportional to the difference between the respective voltages and the offset voltage. The proportionality coefficients were determined based on the best correspondence between the modeled and experimental data. In addition, the electric field in the perovskite layer may be inhomogeneous because ions and trapped charge carriers have a certain distribution near the surfaces of the perovskite layer. For the sake of simplicity and due to the lack of information about the actual distribution of ions and trapped charge carriers, we considered the electric field to be homogeneous. As will be shown in the following, despite such simplifications, a reasonable agreement with the experimental data was obtained, allowing us to understand the main dependencies on the device parameters and the experimental conditions.

The mobilities of electrons and holes were considered to be identical ($\mu_n = \mu_p = \mu$), yielding the same diffusion coefficient $D = \mu k_B T/e$. We also assumed that the recombination rate γ is related to the mobility as $\gamma = q\mu/\varepsilon\varepsilon_0$ (here, $\varepsilon\varepsilon_0$ is electric permittivity of the perovskite layer), as predicted by the Langevin theory. It should be noted that the reported recombination rates for large grain hybrid metal halide perovskites used in solar cells scatter by several orders of magnitude and are typically much slower than predicted by Langevin theory.[30] In contrast, no such information is available for the small-grained perovskites used in the current study. The reported charge carrier mobilities in FAPI perovskites also differ by several orders of magnitude, depending on the material fabrication and the measurement methods.[31] Due to the nanostructured morphology of our perovskites, the carrier motion and recombination properties are expected to be closer to those of low mobility materials described by Langevin theory.

To evaluate these parameters, we first modeled the dependencies of the EL dynamics on the afterpulse voltage. These dependencies are simpler because, as already mentioned, the afterpulse changes only the motion dynamics of the accumulated charge carriers without affecting the accumulation process. Furthermore, the shape of the OSP is determined only by the carrier diffusion when the afterpulse voltage is zero. **Figure 7** shows the modeled room-temperature EL dynamics at an injection voltage of 3 V and an offset voltage of −1.5 V, which was obtained for 40 and 120 nm devices using a dielectric constant $\varepsilon = 20$, a carrier

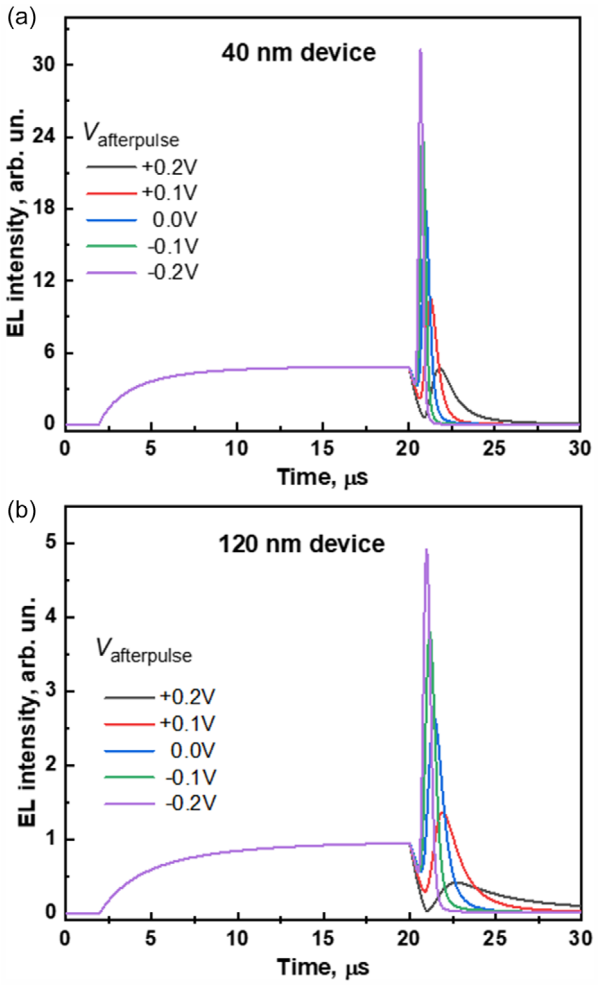

Figure 7. Modeled EL kinetics for a) 40 and b) 120 nm devices driven by 3 V, 20 μs electrical injection pulses under −1.5 V offset voltage at different afterpulse voltages.

mobility of $\mu = 0.002\ cm^2\ V^{-1}s^{-1}$, and other parameters calculated accordingly. The effective internal electric field strength was considered being proportional to the difference between afterpulse and offset voltages. The best agreement with the experimental data was obtained by assuming that the voltage drop on a perovskite layer corresponds to 1/10 of this voltage difference. The simulations successfully reproduced the main dynamic characteristics of the EL and its dependence on the afterpulse voltage. However, the simulated OPSs are slightly shorter than the experimentally observed ones, which also results in the EL decay occurring immediately after the termination of the injection pulse in a 40 nm device and being more pronounced in a 120 nm device. The pulse broadening in the experimental kinetics is most likely caused by the inhomogeneity of the perovskite layer, which was also not taken into account in our simulations. The determined carrier mobility of $0.002\ cm^2\ V^{-1}s^{-1}$ is about 2–3 orders of magnitude lower than the values typically reported for FAPI perovskite. This is not surprising as the perovskites used here are very different from those used in solar cells. The perovskite used in this work consists of small (≈10 nm in diameter) grains covered by electrically insulating organic layers that form barriers to the movement of charge carriers and thus significantly reduce charge carrier mobility.

Next, the determined parameters were used to reproduce the other experimentally obtained data. In our calculations, we used experimentally determined current values. However, dependences of the internal voltage dropping across perovskite layer during the injection pulse action on the injection and offset voltages are very difficult to evaluate. Therefore, the internal voltage was used as a free parameter adjusted to reproduce experimentally determined EL kinetics. As **Figure 8**a,b shows, we were able to quite successfully reproduce the EL kinetics obtained under different injection voltages with −1.5 V offset, as well as their dependencies on the offset voltage presented in Figure 1d. EL dynamics at different applied voltages was quite well simulated just by using experimentally determined currents, while keeping the internal electric field constant. On the other hand, reproduction of the dependence on the offset voltage demanded strong variation of the internal electric field. Thus, the calculations imply that the internal voltage is mainly determined by the offset voltage, consequently by the ionic field, rather than by the injection voltage. We hypothesize that the positive voltage creating strong injection currents mainly drops on the transport layers and interfaces. On the other hand, the negative voltage creates no current therefore voltage drops on insulating perovskite layer causing strong redistribution of ions and consequently strong ionic fields. In agreement with the experimental data, the simulated kinetics show not only the appearance of the OSP signal but also a relatively slow growth of the conventional EL at strong internal electric fields. The modeled EL growth is slightly faster than that observed experimentally. We hypothesize that this is because the growth rate is determined by two processes: charge carrier accumulation and population of trap states, which were not included in our computational model.

Figure 8c shows the spatial distributions of the electron and hole concentrations before the termination of the injection pulse at different internal voltages, which illustrate the initial conditions for the formation of the overshoot. The simulated distributions confirm the qualitative scheme shown in Figure 3. At high values of negative offset, when the electric field inside the perovskite is strong, the electron density (sold lines) is concentrated near the positively charged electrode (anode), while the electron density on the cathode side of the perovskite layer is very low. On this side of the layer, the injected electrons drift under the influence of the strong internal electric field so that their density is

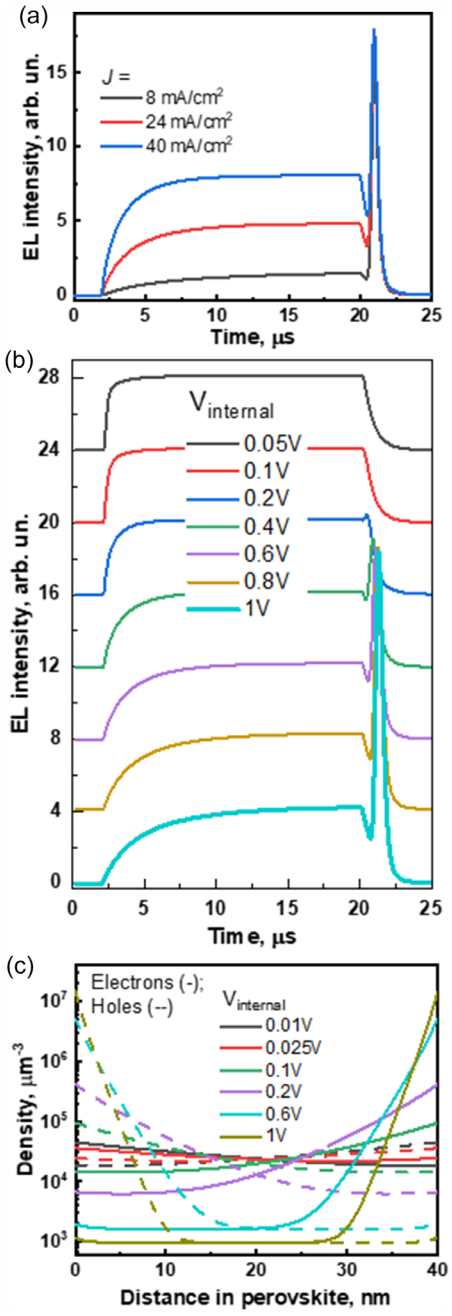

Figure 8. a) Modeled EL dynamics for a 40 nm device driven by different voltages and 20 μs electrical pulses under −1.5 V offset voltage; b) driven by 3 V, 20 μs electrical pulses under different values of internal voltages (for visual clarity, the kinetics were shifted vertically). c) shows steady-state charge carrier density distributions under different values of internal voltage.

approximately inversely proportional to the strength of the electric field. The electron density increases almost exponentially in the direction of the anode. Since it was assumed that the properties of electrons and holes are identical, the distribution of holes is symmetrical with respect to the center of the perovskite layer. This distribution represents the accumulation mode. When the offset voltage is small, zero or positive, the internal electric field becomes weaker, causing more homogeneous, or even reversed distribution of charge carriers, which corresponds to the operation of the device in the recombination mode. Consequently, the modeling confirms the existence of two PeLED performance modes, which are mainly determined by accumulated ions. Two device operation parameters—carrier drift velocity and recombination rate—compete with each other, one favoring the accumulation mode and the other promoting the recombination mode.

3. Discussion

The model presented above and the performed calculations provide valuable insights into the performance of PeLED in both the conventional EL and overshoot regimes. Our simulations show that the efficient simultaneous generation of conventional EL and OSPs is hardly possible, since the efficient generation of conventional EL pulses takes place in the recombination mode, while the formation of OSPs requires the operation of the device in the accumulation mode. The recombination mode is more favorable for the performance of conventional PeLEDs, as the recombination of charge carriers is likely to occur more in the central part of the perovskite layer, where the material quality is typically better, does not contain interfacial trapping and impurity states, and is therefore likely to have a higher luminescence yield. In addition, the accumulation of charge carriers, which leads to their leaking and recombination at the interface, does not occur in this mode or is attenuated.

Competition between drift of charge carriers and their recombination is the main factor determining the operating regime of the PeLED. When recombination of charge carriers is fast, most of them recombine before they cross the perovskite layer, which prevents their accumulation. Slow recombination, on the other hand, allows charge carrier transit through the perovskite layer and their accumulation at the perovskite interfaces. Slow recombination also causes a slow growth of the conventional EL, as the EL intensity increases with the density of the accumulated charge carriers. In case of fast recombination, on the other hand, when PeLED operates in recombination mode, the EL intensity emerges as soon as electrons and holes injected from opposite sides meet each other.

The charge carrier drift velocity is determined by the product of the charge carrier mobility and the strength of internal electric field. We can consider the charge carrier mobility as a material parameter that is independent or only weakly dependent on the device performance conditions but is strongly influenced by the material structure. Our modeling results, along with previous indirect observations,[32] suggest that the carrier mobility in these perovskites is much lower than in conventional large-grained perovskites. This lower mobility enhances PeLED performance in the recombination mode but is not favorable for the formation of overshoot. On the other hand, the individual values of mobility and recombination rate become less important if they are interrelated by the Langevin relation, as it was assumed in our modeling. In this case, the increased recombination rate is compensated by the increased mobility, so that their variations do not change the operation mode. On the other hand, as was mentioned, the Langevin relationship is not necessarily valid.[29]

The strength of the internal electric field under the applied driving voltage is another parameter that determines the charge carrier drift rate and the operation mode of the PeLED. It depends both on the PeLED operation conditions and on the perovskite properties—the thickness of the perovskite layer, the voltage drop across the perovskite layer, and the shielding of the applied electric field by mobile ions and trapped and/or accumulated charge carriers. Increase in the perovskite layer thickness reduces the internal electric field strength and the carrier drift velocity (if the applied voltage remains the same); therefore, it facilitates the PeLED operation in the recombination mode. This is in agreement with the weaker OSPs observed in thicker samples. The densities of the mobile ions and the trap states are also important perovskite parameters. A high concentration of mobile ionic species, such as vacancies and interstitial sites, or a high concentration of charge carrier traps facilitate stronger shielding of the field. On the other hand, the ion distributions and the population of trap states strongly depend on the operation conditions, as shown by the dependencies of the EL intensity and dynamics on the offset voltage, the duration of the injection pulse, and the repetition rate.

The considerations discussed above lead to some insights into the temperature dependence of OSP formation. As discussed above, within the Langevin theory, the recombination rate and carrier mobility are interrelated as $\gamma = e\mu/\varepsilon_0\varepsilon$; thus, their ratio should be independent of temperature. This result is based on the relation between the recombination rate and diffusion coefficient, $\gamma = 4\pi D r_c$, where r_c is the Coulomb attraction radius defined as $r_c = e^2/(4\pi\varepsilon\varepsilon_0 k_B T)$. However, in the case of small-grained perovskites, the recombination radius is expected to be determined by the grain dimensions and not temperature. In this case, $\gamma \propto \mu T$. Therefore, the ratio of the recombination rate and mobility decreases at low temperatures, leading to a change in PeLED performance towards accumulation mode facilitating the formation of the OSP, in agreement with the experimental dependence.

Let us now briefly discuss the potential of OSP in generating short EL pulses with high intensity and high contrast compared to conventional EL. The first task to achieve this goal is to accumulate high concentrations of electrons and holes. The fundamental processes that limit the achievable concentrations of accumulated charge carriers are their leaking and recombination. The leaking of charge carriers can be prevented by the use of effective blocking layers. Thus, although this is a practically important factor, it does not set fundamental limits. However, the recombination rate of charge carriers inevitably increases with the concentration of accumulated charge carriers. We predict two types of recombination processes: the recombination of accumulated electrons with accumulated holes and the recombination of injected charge carriers during their drift through the cloud of accumulated charge carriers of another type. The recombination rate of accumulated elections

with accumulated holes is proportional to the overlap of their spatial distributions. We can reduce this overlap by increasing the internal electric field, which compresses the charge carrier distributions near the opposite electrodes. Stronger internal electric field also reduces the recombination rate of the accumulated and drifting injected carriers because it increases their drift velocity and consequently reduces the time interval required to cross the region of accumulated carriers. The internal electric field can be increased by applying a high voltage. However, as Figure 2 shows, this increases the carrier injection and the conventional EL, while the intensity of the OSP pulses goes into saturation. The reason for the latter effect is probably twofold: 1) the increased leakage of accumulated charge carriers which is proportional to their concentration at the contact and 2) the increased shielding of the applied electric field by the accumulated charge carriers. Another possible approach is the enhancement of the internal electric field created by the accumulated ions using the offset voltage. The offset voltage does not increase the carrier injection and the conventional EL, thus not only reducing the recombination rate but also increasing the ratio of OSP-to-conventional EL.

The idea of achieving high OSP intensity at low injection voltage and current requires a long carrier accumulation time at a low injection rate. However, as shown in Figure 6, longer injection pulses lead to a stronger increase in conventional EL than in OSP intensity and, thus, to a lower ratio of OSP-to-conventional EL. We attribute it to the trapping of the accumulated charge carriers. This process could probably be mitigated by reducing the density of trap states.

The generation of short OSPs with high intensity also requires rapid recombination of the accumulated charge carriers when the injection pulse terminates. This process is determined by the carrier diffusion and recombination rates. As we demonstrated, one can partly control it by applying afterpulse voltage. The simulations show that certain device and operation parameters should allow the generation of high-intensity pulses with a very large ratio of OSP to conventional EL. Thus, within our model accounting major processes determining overshoot formation, there are no fundamental limits on the intensity of the OSP and its ratio to the conventional EL intensity. However, additional processes, such as carrier leakage, or Auger recombination, not included into our model apparently set limits. In our devices, they caused experimentally observed OSP to conventional EL ratio up to about 10. Special device optimization apparently may help to increase this ratio and to reach higher OSP intensities. We demonstrate this for PeLED while driving with relatively low voltage pulses of several volts and current densities of up to hundreds of mA/cm^{-2}. However, this conclusion is not necessarily valid for the PeLED while driving at very high current densities with voltages of hundreds of volts when attempting to generate conventional EL pulses of very high intensity, such as those required for electrically pumped lasers. Some processes may change qualitatively under these operation conditions.

4. Conclusions

The overshoot effect in perovskite LEDs (PeLEDs) enables the generation of short high-intensity light pulses when the PeLEDs are driven by longer low-voltage pulses. Here, we analyze the formation of OSP under different operation conditions in small-grain FAPI PeLEDs of different thicknesses. We demonstrate two operation modes: the recombination mode, which ensures high efficiency in the conventional EL but prevents the formation of OSP, and the accumulation mode, which allows the formation of OSP but is less favorable for the conventional EL. The operation mode is determined by the competition between the transfer of injected charge carriers through the perovskite layer and their recombination. Thus, it is governed by two important material parameters—the charge carrier mobility and the recombination rate—as well as the internal electric field. The strength of the electric field is determined not only by the injection voltage but also by the distribution of mobile ions and the population of trap states. The ion distribution can be controlled by applying an offset voltage between the injection pulses, which suggests an effective way to control the operation mode of the PeLED. Mathematical modeling shows that within the used model accounting for major carrier motion and recombination processes, there are no fundamental restrictions on the OSP intensity. However, additional processes, not included into or model, apparently set limitations, particularly at high driving voltages. The desire of prominent OSP parameters requires optimization of carrier mobility, reduction of carrier trap densities, and effective prevention of carrier leakage.

5. Experimental Section

PeLED Fabrication: The perovskite layers were fabricated to be composed of small perovskite grains with a diameter of 10–30 nm, as suggested by Xiao et al.[33] The structure and fabrication of the devices have been described elsewhere.[26] In brief, the devices were fabricated on pre-patterned ITO glass substrates. A 15 nm polyTPD hole transport layer was formed by spin coating, which was then annealed at 150 °C for 20 min and treated with O_2 plasma for 6 s to improve surface wettability. Subsequently, PbI_2 and FAI were dissolved in DMF with 20 mol% additional benzylammonium iodide in a N_2 glove box, using an antisolvent method to form a small-grained perovskite layer. A PCBM solution in chlorobenzene was then deposited to form a 20 nm layer, followed by deposition of a 20 nm-thick layer of ZnMgO nanoparticles. The devices with an area of 0.125 cm^2 were finalized by thermal evaporation of 100 nm Al through the shadow mask.

Investigation Equipment: The EL dynamics of PeLEDs was detected by the Hamamatsu photomultiplier H6780-20. Electrical driving was performed at 6.6 Hz frequency by means of the function generator Tektronix AFG 3101. Electrical signals were recorded by a 500 MHz Agilent Technologies oscilloscope DSO5054A.

Acknowledgements

This work was partly financed by the Research Council of Lithuania under grant agreement P-MIP-24-77 and partially by the European Research Council under the European Horizon 2020 Programme/ERC grant agreement No. 835133 (ULTRA-LUX).

Conflict of Interest

The authors declare no conflict of interest.

Data Availability Statement

The data that support the findings of this study are available from the corresponding author upon reasonable request.

Keywords

electroluminescence, ion redistribution, overshoot, PeLED

Received: July 2, 2025
Revised: September 19, 2025
Published online:

[1] L. Zhang, L. Mei, K. Wang, Y. Lv, S. Zhang, Y. Lian, X. Liu, Z. Ma, G. Xiao, Q. Liu, S. Zhai, *Nano-Micro Lett.* **2023**, *15*, 177.
[2] Q. V. Le, H. W. Jang, S. Y. Kim, *Small Methods* **2018**, *2*, 1700419.
[3] D. Yang, B. Zhao, T. Yang, R. Lai, D. Lan, R. H. Friend, D. Di, *Adv. Funct. Mater.* **2021**, *32*, 2109495.
[4] J. Chen, H. Xiang, J. Wang, R. Wang, Y. Li, Q. Shan, X. Xu, Y. Dong, C. Wei, H. Zeng, *ACS Nano* **2021**, *15*, 17150.
[5] Z. Ren, K. Wang, X. W. Sun, W. C. H. Choy, *Adv. Funct. Mater.* **2021**, *31*, 2100516.
[6] K. Lin, J. Xing, L. N. Quan, F. P. G. de Arquer, X. Gong, J. Lu, L. Xie, W. Zhao, D. Zhang, C. Yan, W. Li, X. Liu, Y. Lu, J. Kirman, E. H. Sargent, Q. Xiong, Z. Wei, *Nature* **2018**, *562*, 245.
[7] S. Xing, Y. Yuan, G. Zhang, S. Zhang, Y. Lian, W. Tang, K. Zhou, S. Liu, Y. Gao, Z. Ren, G. Zhang, T. Sun, B. Zhao, D. Di, *ACS Energy Lett.* **2024**, *9*, 3643.
[8] J. S. Kim, J. M. Heo, G. S. Park, S. J. Woo, C. Cho, H. J. Yun, D. H. Kim, J. Park, S. C. Lee, S. H. Park, E. Yoon, N. C. Greenham, T. W. Lee, *Nature* **2022**, *611*, 688.
[9] W. Bai, T. Xuan, H. Zhao, H. Dong, X. Cheng, L. Wang, R. J. Xie, *Adv. Mater.* **2023**, *35*, 2302283.
[10] Z. Liu, W. Qiu, X. Peng, G. Sun, X. Liu, D. Liu, Z. Li, F. He, C. Shen, Q. Gu, F. Ma, H. L. Yip, L. Hou, Z. Qi, S. J. Su, *Adv. Mater.* **2021**, *33*, 2103268.
[11] C. Zou, Y. Liu, D. S. Ginger, L. Y. Lin, *ACS Nano* **2020**, *14*, 6076.
[12] K. Elkhouly, I. Goldberg, X. Zhang, N. Annavarapu, S. Hamdad, G. Croes, C. Rolin, J. Genoe, *Nat. Photonics* **2024**, *18*, 132.
[13] K. Sim, T. Jun, J. Bang, H. Kamioka, J. Kim, H. Hiramatsu, H. Hosono, *Appl. Phys. Rev.* **2019**, *6*, 031402-1.
[14] R. Gegevičius, M. Franckevičius, J. Chmeliov, W. Tress, V. Gulbinas, *J. Phys. Chem. Lett.* **2019**, *10*, 1779.
[15] J. M. Lupton, V. R. Nikitenko, I. D. W. Samuel, H. Bässler, *J. Appl. Phys.* **2001**, *89*, 311.
[16] V. R. Nikitenko, V. I. Arkhipov, Y. H. Tak, J. Pommerehne, H. Bässler, H. H. Hörhold, *J. Appl. Phys.* **1997**, *81*, 7514.
[17] A. Fakharuddin, W. Qiu, G. Croes, A. Devižis, R. Gegevičius, A. Vakhnin, C. Rolin, J. Genoe, R. Gehlhaar, A. Kadashchuk, V. Gulbinas, P. Heremans, *Adv. Funct. Mater.* **2019**, *29*, 1904101.
[18] M. A. Torre Cachafeiro, N. K. Kumawat, F. Gao, W. Tress, *Natl. Sci. Rev.* **2025**, *12*, nwae128.
[19] K. Elkhouly, I. Goldberg, H.-G. Boyen, A. Franquet, V. Spampinato, T.-H. Ke, R. Gehlhaar, J. Genoe, J. Hofkens, P. Heremans, W. Qiu, *Adv. Opt. Mater.* **2021**, *9*, 2100586.
[20] J. Chmeliov, K. Elkhouly, R. Gegevičius, L. Jonušis, A. Devižis, A. Gelžinis, M. Franckevičius, I. Goldberg, J. Hofkens, P. Heremans, W. Qiu, V. Gulbinas, *Adv. Opt. Mater.* **2021**, *9*, 2101560.
[21] R. Gegevičius, K. Elkhouly, M. Franckevičius, J. Chmeliov, I. Goldberg, R. Gehlhaar, W. Qiu, J. Genoe, P. Heremans, V. Gulbinas, *ACS Appl. Mater. Interfaces* **2023**, *15*, 42784.
[22] D. Cao, Y. Wang, *J. Phys. Chem. Lett.* **2024**, *15*, 6986.
[23] N. K. Kumawat, W. Tress, F. Gao, *Nat. Commun.* **2021**, *12*, 4899.
[24] D. Luo, Q. Chen, Y. Qiu, M. Zhang, B. Liu, *Nanomaterials* **2019**, *9*, 1007.
[25] Y. Sun, S. Chen, J.-Y. Huang, Y.-R. Wu, N. C. Greenham, *Appl. Phys. Rev.* **2024**, *11*, 041418.
[26] K. Elkhouly, I. Goldberg, N. Annavarapu, R. Gehlhaar, T. H. Ke, J. Genoe, J. Hofkens, P. Heremans, W. Qiu, *Adv. Opt. Mater.* **2022**, *10*, 2200024.
[27] I. Allegro, Y. Li, B. S, Richards, U. W. Paetzold, U. Lemmer, I. A. Howard, *J. Phys. Chem. Lett.* **2021**, *12*, 2293.
[28] Y. He, J. Yan, L. Xu, B. Zhang, Q. Cheng, Y. Cao, J. Zhang, C. Tao, Y. Wei, K. Wen, Z. Kuang, G. M. Chow, Z. Shen, Q. Peng, W. Huang, J. Wang, *Adv. Mater.* **2021**, *33*, 2006302.
[29] R. L. Milot, G. E. Eperon, H. J. Snaith, M. B. Johnston, L. M. Herz, *Adv. Funct. Mater.* **2015**, *25*, 6218.
[30] M. B. Johnston, L. M. Herz, *Acc. Chem. Res.* **2016**, *49*, 146.
[31] L. M. Herz, *ACS Energy Lett.* **2017**, *2*, 1539.
[32] K. Elkhouly, M. Franckevičius, V. Jašinskas, A. Gelžinis, I. Goldberg, R. Gehlhaar, J. Genoe, P. Heremans, V. Gulbinas, *ACS Appl. Mater. Interfaces* **2025**, *17*, 9625.
[33] Z. Xiao, R. A. Kerner, L. Zhao, N. L. Tran, K. M. Lee, T. W. Koh, G. D. Scholes, B. P. Rand, *Nat. Photonics* **2017**, *11*, 108.

